

# Plasmonic Toroidal Metamolecules Assembled by DNA Origami

Maximilian J. Urban,<sup>†</sup> Palash K. Dutta,<sup>‡</sup> Pengfei Wang,<sup>‡</sup> Xiaoyang Duan,<sup>†</sup> Xibo Shen,<sup>†</sup> Baoquan Ding,<sup>\*,§</sup> Yonggang Ke,<sup>\*,‡</sup> and Na Liu<sup>\*,†,||</sup>

<sup>†</sup>Max Planck Institute for Intelligent Systems, D-70569 Stuttgart, Germany

<sup>‡</sup>Wallace H. Coulter Department of Biomedical Engineering, Georgia Institute of Technology and Emory University, Atlanta, Georgia 30322, United States

<sup>§</sup>CAS Key Laboratory of Nanosystems and Hierarchical Fabrication, CAS Center for Excellence in Nanoscience, National Center for Nanoscience and Technology, Beijing 100190, China

<sup>||</sup>Kirchhoff Institute for Physics, University of Heidelberg, D-69120 Heidelberg, Germany

## Supporting Information

**ABSTRACT:** We show hierarchical assembly of plasmonic toroidal metamolecules that exhibit tailored optical activity in the visible spectral range. Each metamolecule consists of four identical origami-templated helical building blocks. Such toroidal metamolecules show a stronger chiroptical response than monomers and dimers of the helical building blocks. Enantiomers of the plasmonic structures yield opposite circular dichroism spectra. Experimental results agree well with the theoretical simulations. We also show that given the circular symmetry of the structures a distinct chiroptical response along their axial orientation can be uncovered via simple spin-coating of the metamolecules on substrates. Our work provides a new strategy to create plasmonic chiral platforms with sophisticated nanoscale architectures for potential applications such as chiral sensing using chemically based assembly systems.

Realization of 3D plasmonic nanoarchitectures exemplifies one of the key challenges in nanotechnology.<sup>1</sup> There are two basic types of nanofabrication strategies: top-down and bottom-up. Top-down approaches such as electron-beam lithography and focused-ion beam etching offer custom patterns with relatively low throughput and resolution.<sup>2</sup> Fabricated 3D plasmonic nanostructures are generally fashioned in layers and spaced with dielectrics. This poses many challenges for downstream applications. However, bottom-up self-assembly approaches<sup>3</sup> that often involve molecular recognition characters, offer large-scale fabrication and biochemical compatibility among other benefits. Among a variety of materials for self-assembly, DNA is one of the most attractive building blocks largely because of its unprecedented programmability. DNA has been used to construct increasingly complex structures<sup>4</sup> and to pattern nanoparticles.<sup>5</sup> The DNA origami<sup>4</sup> technique allows for creation of fully addressable DNA templates with custom-designed shapes and sizes. DNA origami enables rational 3D organization of metal nanoparticles with nanometer precision, allowing for engineering complex plasmonic architectures with tailored optical response.

Plasmonic chiral nanomaterials have gained increasing attention because of their potential applications in nanophotonics and ultrasensitive sensing and others.<sup>6</sup> Natural chiral

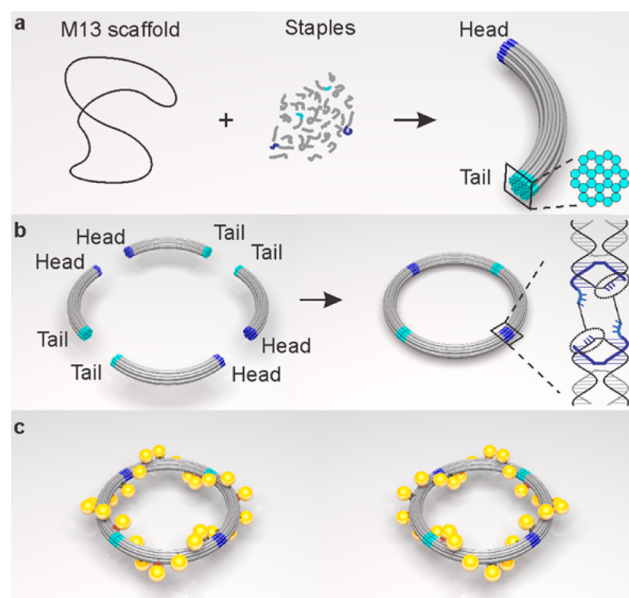


**Figure 1.** (a) Curved DNA origami monomer that comprises 24 DNA helices in a bundle is formed by a scaffold strand and numerous staple strands. (b) Four origami monomers form an origami ring through head–head and tail–tail connectors. (c) Schematic of the left- and right-handed 3D plasmonic toroidal metamolecules. Each metamolecule has a toroidal diameter of 120 nm and consists of 24 AuNPs (13 nm).

molecules such as proteins and DNA only exhibit weak optical activity in the UV range. Plasmonic assemblies composed of metal nanoparticles arranged in chiral configurations offer an elegant way to achieving strong optical activity in the visible spectral range<sup>6</sup> (e.g., in the seminal work of Liedl et al., plasmonic helices were realized by assembling gold nanoparticles (AuNPs) on origami bundles in a staircase fashion).<sup>7</sup> Nevertheless, previous work has mostly focused on studies of fundamental plasmonic chiral building blocks (e.g., helices<sup>7</sup> and tetramers<sup>8</sup>) and averaged chiroptical response over all structural orientations because the assemblies were randomly oriented in aqueous solutions.

Received: January 27, 2016

Published: April 15, 2016

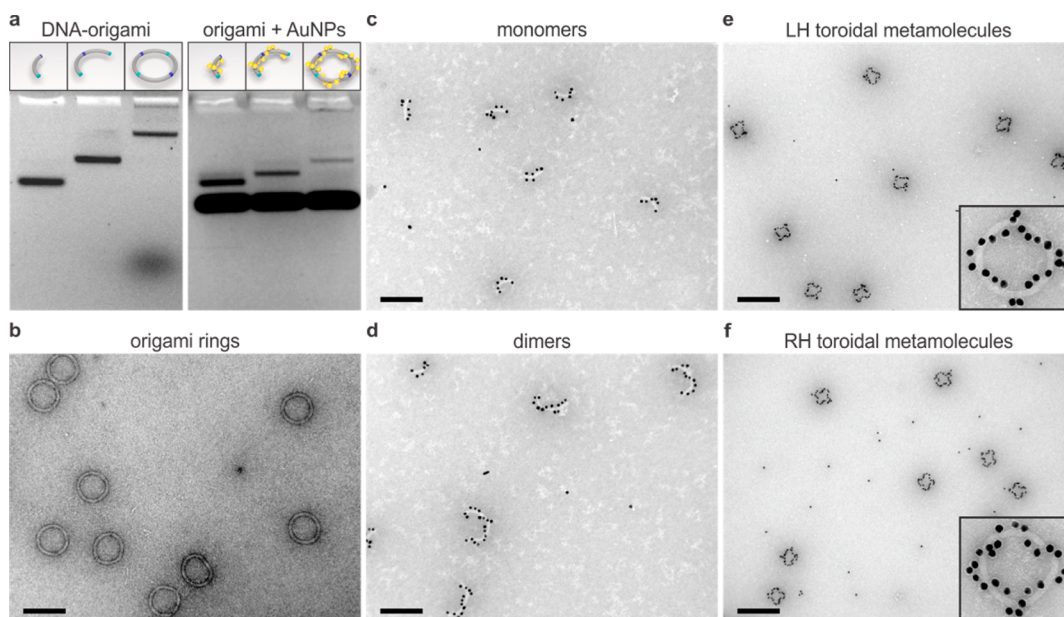


**Figure 2.** (a) Left: Agarose gel electrophoresis images of the origami monomers, dimers, and rings. Right: Agarose gel electrophoresis images of the plasmonic LH helical monomers, dimers, and toroidal metamolecules. (b) TEM image of the origami rings (scale bar 200 nm). (c) TEM image of the LH plasmonic helical monomers (scale bar 200 nm). (d) TEM image of the LH plasmonic helical dimers (scale bar 200 nm). TEM images of the (e) LH and (f) RH plasmonic toroidal metamolecules (scale bar 400 nm). Frame size of each inset image is 200 nm.

Here we show the first experimental realization of plasmonic toroidal metamolecules through hierarchical assembly of helical building blocks templated by DNA origami. Each structure consists of four plasmonic helical monomers arranged in a toroidal geometry.<sup>9</sup> Systematic investigations on different experimental conditions are carried out to achieve high-quality plasmonic structures for tailored optical functionalities. Assembled metamolecules with designated handedness exhibit pronounced optical activity in the visible spectral range. Experimental optical spectra agree well with the theoretical predictions. We also show that given the unique circular symmetry distinct chiroptical response along the axial orientation of the toroidal metamolecules can be revealed by simple spin-coating of the structures on substrates. Such orientation self-alignment neither requires surface functionalization nor introduces birefringence effects that often arise from symmetry breaking. This is of great importance for achieving reliable chiroptical results on the single-structure level using dark-field spectroscopy and is very practical for development of polarization conversion devices using chemically based assembly systems. In addition, the axial chiroptical response can be enhanced through Ag coating of the AuNP-based structures. Elemental mapping with energy-filtered TEM clearly shows the formation of Au core/Ag shell nanoparticles in a toroidal geometry.

Plasmonic toroidal metamolecules are assembled utilizing the DNA origami technique (Figure 1). A long single-stranded DNA scaffold (M13 bacteriophage DNA) is folded by  $\sim 180$  short staple strands through hybridization to form an origami monomer (Figures 1a, S1, and S2; see also Supporting Information for more design details). Each monomer contains 24 curved DNA helices bundled in a honeycomb lattice.<sup>10</sup> Four monomers are connected together using 12 head–head and 12 tail–tail connector strands to form a complete origami ring of  $\sim 120$  nm in terms of inner diameter (Figures 1b and S3). Half-ring structures (i.e., dimers) can be achieved by linking two monomers using either the head–head or tail–tail connectors. To assemble AuNPs on origami, six binding sites arranged either

in left-handed (LH) or right-handed (RH) fashion are extended from each monomer. Each binding site contains three capture strands of the same sequence. Overall, 24 binding sites are distributed evenly along 1 complete origami ring. To ensure that each AuNP binds only to one site, two sets of capture strands with different sequences are used for the binding sites on the monomers in an alternating fashion. AuNPs (13 nm in diameter) functionalized with complementary DNA strands are assembled onto the origami ring to form a LH or RH plasmonic toroidal metamolecule (Figure 1c).

Previously, Shih et al. have shown a gearlike origami structure of  $\sim 100$  nm in diameter using four 18-helix homomonomers, but the yield was lower than 10%.<sup>11</sup> To ensure a high yield of our origami rings, critical to create high-quality plasmonic structures for strong chiroptical response, careful optimization of the ring design and assembly protocol have been carried out. First, we tested two versions (V1 and V2) of monomer designs with different degrees of curvatures (Figures S1–S7). Mean angles of the V1 and V2 monomers are  $99 \pm 9$  and  $79 \pm 12^\circ$ , respectively (Figure S7). V1 monomers show higher yield for forming origami rings, whereas the V2 monomers give rise to mainly larger concatemers. Hence, subsequent optimization has been carried out using the V1 origami.

Second, the influence from the sticky-end strength of the connectors on the hierarchical assembly<sup>12</sup> of the origami rings is investigated. Each connector comprises two segments. One segment is anchored on the edge of one monomer, and the other segment that contains 12 sticky ends (either 1 or 3 bases long) is anchored on the edge of another monomer. Systematic studies using gel electrophoresis and TEM clearly show that connectors with 3 base long sticky ends give rise to higher yield than those with 1 base long sticky ends (Figure S8a). Stronger sticky ends with higher binding forces may minimize nonspecific binding and thus facilitate the formation of the origami rings.

A comparison between the rings formed either directly or in a stepwise manner from purified monomers and the rings formed from purified dimers shows no substantial difference in yield

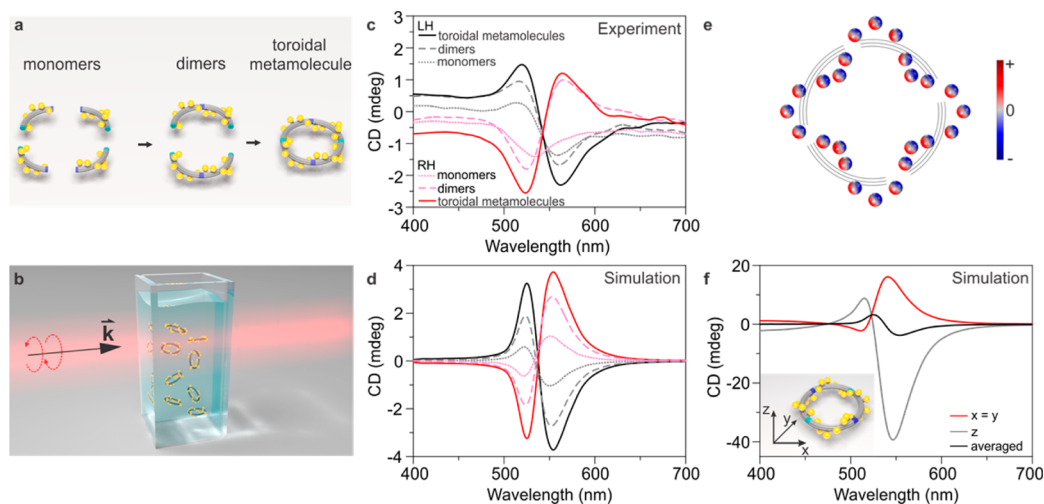


**Figure 3.** (a) Stepwise formation of the plasmonic toroidal metamolecules. (b) Schematic for the CD measurement of the plasmonic nanostructures that are dispersed in water with random orientations. (c) Measured and (d) simulated CD spectra of the plasmonic helical monomers, dimers, and toroidal metamolecules. (e) Charge distribution ( $E_z$ ) of the plasmonic structure at resonance. (f) CD components of the LH plasmonic toroidal metamolecules along different incident directions of the circularly polarized light. Black curve, averaged CD response.

(Figure S8b). Last, the effects of the dimer concentration, assembly time, and connector strand concentration on the assembly yield of the origami rings are examined (Figures S9 and S10). Experimental results show that lower dimer concentrations (0.4 and 0.2 nM) lead to significantly improved yield ( $\sim 49$  and  $\sim 67\%$ , respectively) of the origami rings, when compared to 32% from a higher dimer concentration of 1 nM. Incorrect assemblies are mostly aggregated spiral-like structures as observed from gel electrophoresis and TEM images (Figure S9). Lower assembly concentrations are associated with slower assembly rates and lower possibilities of aggregation that could both contribute to higher yield of the origami rings. In another experiment on various assembly times, many incomplete rings are observed when incubation time is  $< 6$  h (Figure S10a). Structure analysis using gel electrophoresis shows that a minimal 50-fold excess of the connectors is required to achieve a high yield of the origami rings (Figure S10b). Utilizing the optimized design and assembly protocol, DNA origami monomers, dimers, and rings are successfully assembled with high yield, as confirmed by gel electrophoresis (Figure 2a, left panel) and TEM imaging (Figure 2b). Inner diameter of the rings is measured to be  $120.0 \pm 3.9$  nm based TEM images (Figure S11). Plasmonic helical monomers, dimers and toroidal metamolecules in LH and RH geometries are assembled via attaching AuNPs onto the origami precursors. AuNPs functionalized with single-stranded DNA are mixed with the corresponding purified origami at a 10-fold excess of particles per binding site. Both gel electrophoresis (Figure 2a, right panel) and TEM images (Figures 2c–f) confirm the successful assembly of the plasmonic nanostructures (Figure S12). Plasmonic toroidal structures were purified by gel electrophoresis prior to TEM imaging (Figure 2e,f). Particle numbers fewer than 24 are observed from the individual plasmonic structures. This is likely due to steric hindrance between the AuNPs and the inner-capture strands that are less accessible than the outer ones (Figure S13).

When interacting with light, plasmons excited in the AuNPs can be collectively coupled.<sup>6</sup> Helical arrangement of the AuNPs imprints a “corkscrew” character to the collective plasmons, introducing a twist of specific handedness into the propagation direction of light, leading to different absorption in response to

LH and RH circularly polarized light (i.e., circular dichroism (CD)).

To characterize the chiroptical response of the plasmonic helical monomers, dimers, and toroidal metamolecules, CD measurements have been carried out using a Jasco-1500 CD spectrometer. To keep the AuNP concentration in all measurements consistent, the CD spectra are measured from the same solution first by adding head–head connectors into monomers to form dimers and subsequently by adding the tail–tail connectors to form toroidal metamolecules (Figure 3a,b). LH monomers, dimers, and toroidal metamolecules exhibit characteristic peak-

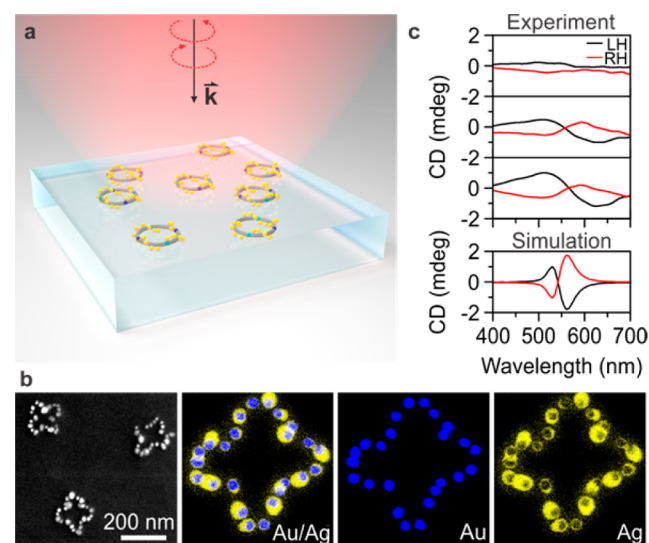


**Figure 4.** (a) Schematic for the axial CD component measurement of the plasmonic toroidal metamolecules. Circularly polarized light is perpendicularly incident on the structures. (b) Left: SEM image of the toroidal metamolecules after Ag enhancement. Right: Energy-filtered TEM images of the Ag-enhanced metamolecules. Blue and yellow represent Au and Ag, respectively. Frame size: 205 nm. (c) Measured and simulated CD spectra of the LH and RH samples after 1 (top), 3 (middle), and 10 (bottom) spin-coating cycles of the respective structures on the glass substrates. Structure density after 10 spin coating cycles increased to  $\sim 0.15$  ring/ $\mu\text{m}^2$ , also utilized in the simulations.



to-dip line shapes with increasing amplitudes, whereas their RH counterparts display mirrored spectra correspondingly. Plasmonic toroidal metamolecules show the most pronounced CD spectra when compared to the constituent plasmonic helical monomers and dimers (Figures 3c and S14). Experimental results agree well with the simulated results (Figure 3d). Charge distribution at resonance (Figure 3e) shows clearly the dipole coupling nature between the neighboring AuNPs. In the aqueous solution, the plasmonic metamolecules are randomly oriented and illuminated by light of fixed incident direction (Figure 3b). In simulations, this is equivalent to averaging over the CD components along all possible incident directions. Figure 3f gives the simulated CD components along different directions and the averaged CD response of the LH plasmonic toroidal metamolecules.

Next, the CD response along the axial orientation of the toroidal metamolecules is explored by spin-coating the respective LH and RH structures on glass substrates after Ag enhancement. Incident direction of light is perpendicular to the substrate; the axial CD component of the structures becomes accessible (Figure 4a). Ag enhancement is utilized to achieve enhanced CD signals using a relatively small amount of the structures (Figure S15). Deposition of Ag shells on the AuNPs in the assemblies is verified by scanning electron microscopy (SEM) imaging and elemental mapping imaging using energy-filtered TEM (Figure 4b). LH or RH sample (1.5  $\mu\text{L}$ ) is first spin-coated on a glass substrate at 4000 rpm, yielding a very weak CD response (Figure 4c, top panel), owing to a low structure density of  $<0.1$  rings/ $\mu\text{m}^2$  (Figure S16). Through repetitive spin-coatings, the structure density is eventually increased to  $\sim 0.15$  ring/ $\mu\text{m}^2$  (bottom); thus, the CD response becomes increasingly stronger. LH and RH samples exhibit bisignate spectral profiles that are nearly mirrored (Figure 4c). Experimental spectra show broader spectral profiles when compared to the simulated spectra (Figure 4c) because of inhomogeneous broadening mainly resulting from the Ag shell thickness variations over different AuNPs. However, a uniform Ag shell (5 nm) over different AuNPs is utilized in the simulations. Spin-coating and drying may also cause distortion to the toroidal geometry. Elimination of birefringence effects is confirmed by measuring all the samples from the front and back incident directions (Figure S17). Simulations on toroidal dimer structures and fused toroidal structures are shown in Figures S18 and S19, respectively.

We showed DNA-origami-templated plasmonic toroidal metamolecules that yield tailored optical activity in the visible spectral range. Plasmonic toroidal metamolecules show a stronger chiroptical response than the constituent plasmonic chiral building blocks such as helical monomers and dimers. Toroidal metamolecules can be dispersed on solid substrates for generating chiroptical response along their axial orientation. This might offer a new pathway to create plasmonic platforms with tunable CD for enantiomer sensing. CD intensity dependence on the structure density could also be useful for development of polarization conversion devices, allowing for specific polarizations of light with controlled intensities.

## ■ ASSOCIATED CONTENT

### 📄 Supporting Information

The Supporting Information is available free of charge on the ACS Publications website at DOI: 10.1021/jacs.6b00958.

Experimental details. (PDF)

## ■ AUTHOR INFORMATION

### Corresponding Authors

\*dingbq@nanoctr.cn

\*yonggang.ke@emory.edu

\*laura.liu@is.mpg.de

### Author Contributions

M.J.U., P.K.D., and P.W. contributed equally to this work.

### Notes

The authors declare no competing financial interest.

## ■ ACKNOWLEDGMENTS

We thank K. Hahn for assistance with elemental mapping and HR-TEM microscopy. TEM data was collected at the Stuttgart Center for Electron Microscopy (StEM). We thank T. Weiss and A. Asenjo-Garcia for initial calculations. This research was supported by the Sofja Kovalevskaja grant from the Alexander von Humboldt-Foundation, the Marie Curie CIG grant, and the European Research Council (ERC Dynamic Nano) grant. We also acknowledge support from the Wallace H. Coulter Department of Biomedical Engineering Faculty Startup Grant and a Winship Cancer Institute Billi and Bernie Marcus Research Award.

## ■ REFERENCES

- (1) Liu, Y.; Zhang, X. *Chem. Soc. Rev.* **2011**, *40*, 2494–2507.
- (2) Soukoulis, C. M.; Wegener, M. *Nat. Photonics* **2011**, *5*, 523–530.
- (3) Jones, M. R.; Osberg, K. D.; Macfarlane, R. J.; Langille, M. R.; Mirkin, C. A. *Chem. Rev.* **2011**, *111*, 3736–3827.
- (4) Rothmund, P. W. *Nature* **2006**, *440*, 297–302.
- (5) (a) Pinheiro, A. V.; Han, D.; Shih, W. M.; Yan, H. *Nat. Nanotechnol.* **2011**, *6*, 763–772. (b) Topping, T.; Voigt, N. V.; Nangreave, J.; Yan, H.; Gothelf, K. V. *Chem. Soc. Rev.* **2011**, *40*, 5636–5646. (c) Li, Y.; Liu, Z.; Yu, G.; Jiang, W.; Mao, C. *J. Am. Chem. Soc.* **2015**, *137*, 4320–4323. (d) Tian, Y.; Wang, T.; Liu, W.; Xin, H. L.; Li, H.; Ke, Y.; Shih, W. M.; Gang, O. *Nat. Nanotechnol.* **2015**, *10*, 637–644. (e) Lan, X.; Lu, X.; Shen, C.; Ke, Y.; Ni, W.; Wang, Q. *J. Am. Chem. Soc.* **2015**, *137*, 457–462. (f) Sharma, J.; Chhabra, R.; Liu, Y.; Ke, Y.; Yan, H. *Angew. Chem., Int. Ed.* **2006**, *45*, 730–735.
- (6) (a) Fan, Z.; Govorov, A. O. *Nano Lett.* **2010**, *10*, 2580–2587. (b) Zhou, C.; Duan, X.; Liu, N. *Nat. Commun.* **2015**, *6*, 8102. (c) Urban, M. J.; Zhou, C.; Duan, X.; Liu, N. *Nano Lett.* **2015**, *15*, 8392–8396.
- (7) Kuzyk, A.; Schreiber, R.; Fan, Z.; Pardatscher, G.; Roller, E. M.; Hoge, A.; Simmel, F. C.; Govorov, A. O.; Liedl, T. *Nature* **2012**, *483*, 311–314.
- (8) (a) Shen, X.; Asenjo-Garcia, A.; Liu, Q.; Jiang, Q.; Garcia de Abajo, F. J.; Liu, N.; Ding, B. *Nano Lett.* **2013**, *13*, 2128–2133. (b) Mastroianni, A. J.; Claridge, S. A.; Alivisatos, A. P. *J. Am. Chem. Soc.* **2009**, *131*, 8455–8459.
- (9) Kaelberer, T.; Fedotov, V. A.; Papasimakis, N.; Tsai, D. P.; Zheludev, N. I. *Science* **2010**, *330*, 1510–1512.
- (10) Douglas, S. M.; Marblestone, A. H.; Teerapittayanon, S.; Vazquez, A.; Church, G. M.; Shih, W. M. *Nucleic Acids Res.* **2009**, *37*, 5001–5006.
- (11) Dietz, H.; Douglas, S. M.; Shih, W. M. *Science* **2009**, *325*, 725–730.
- (12) (a) Liu, W.; Zhong, H.; Wang, R.; Seeman, N. C. *Angew. Chem., Int. Ed.* **2011**, *50*, 264–267. (b) Li, Z.; Liu, M.; Wang, L.; Nangreave, J.; Yan, H.; Liu, Y. *J. Am. Chem. Soc.* **2010**, *132*, 13545–13552. (c) Rajendran, A.; Endo, M.; Katsuda, Y.; Hidaka, K.; Sugiyama, H. *ACS Nano* **2011**, *5*, 665–671. (d) Iinuma, R.; Ke, Y.; Jungmann, R.; Schlichthaerle, T.; Woehrstein, J. B.; Yin, P. *Science* **2014**, *344*, 65–69. (e) Jungmann, R.; Scheible, M.; Kuzyk, A.; Pardatscher, G.; Castro, C. E.; Simmel, F. C. *Nanotechnology* **2011**, *22*, 275301. (f) He, Y.; Ye, T.; Su, M.; Zhang, C.; Ribbe, A. E.; Jiang, W.; Mao, C. *Nature* **2008**, *452*, 198–201.